Characterization and Development of Universal Ventricular Assist Device: Computational Fluid Dynamics Analysis of Advanced Design

Mark S. Goodin*, Michael S. Showalter†, David J. Horvath‡, Barry D. Kuban§, Christine R. Flick§, Anthony R. Polakowski§, Kiyotaka Fukamachi§,¶ and Jamshid H. Karimov§,¶

We are developing a universal, advanced ventricular assist device (AVAD) with automatic pressure regulation suitable for both left and right ventricular support. The primary goal of this computational fluid dynamics (CFD) study was to analyze the biventricular performance of the AVAD across its wide range of operating conditions.

An AVAD CFD model was created and validated using *in vitro* hydraulic performance measurements taken over conditions spanning both left ventricular assist device (LVAD) and right ventricular assist device (RVAD) operation. Static pressure taps, placed throughout the pump, were used to validate the CFD results. The CFD model was then used to assess the change in hydraulic performance with varying rotor axial positions and identify potential design improvements. The hydraulic performance was simulated and measured at rotor speeds from 2,300 to 3,600 revolutions/min and flow rates from 2.0 to 8.0 L/min. The CFD-predicted hydraulic pressure rise agreed well with the *in vitro* measured data, within 6.5% at 2300 rpm and within 3.5% for the higher rotor speeds. The CFD successfully predicted wall static pressures, matching experimental values within 7%. High degree of similarity and circumferential uniformity in the pump's flow fields were observed over the pump operation as an LVAD and an RVAD. A secondary impeller axial clearance reduction resulted in a 10% decrease in peak flow residence time and lower static pressures on the secondary impeller. These lower static pressures suggest a reduction in the upwards rotor forces from the secondary impeller and a desired increase in the pressure sensitivity of the pump.

The CFD analyses supported the feasibility of the proposed AVAD's use as an LVAD or an RVAD, over a wide range of operating conditions. The CFD results demonstrated the operability of the pump in providing the desired circumferential flow similarity over the intended range of flow/speed conditions and the intended functionality of the AVAD's automated pressure regulation. *ASAIO Journal* 2022; 68;1024–1035

Keywords: heart failure, blood pump, computational fluid dynamics, ventricular assist device, right ventricular assist device, left ventricular assist device, universal VAD, device mapping

Introduction

Heart failure is a serious health issue and a primary contributor to cardiovascular mortality that affects approximately 26 million people worldwide.[1] The incidence of heart failure is also rising rapidly in developing nations. Heart transplantation can provide a remarkable improvement in quality of life and survival in selected patients with end-stage heart disease,[2,3] but a shortage of donor's hearts currently limits this option.[4] In the United States, an estimated 50,000–100,000 patients are in need of heart transplantation or mechanical circulatory support (MCS), but transplantation is performed in only ~2,300 cases per year. Instead, such support is usually provided by left ventricular assist devices (LVADs), the most widely used means for improving the hemodynamic status of both transplant-eligible and noneligible patients.[3] The rate of patient enrollment has grown to exceed 2,500 implants per year for durable mechanical circulatory assist devices such as LVADs and total artificial hearts (TAHs). Device strategy is changing such that the number of LVADs implanted as destination therapy has continued to grow. However, as support duration increases, clinical limitations, and specific complications of LVADs have become apparent. These include a loss of arterial pulsatility,[4,5] development of aortic regurgitation,[5] pump thrombosis or hemolysis,[6,7] severe backflow during pump stoppage, difficulty evaluating native heart function and weanability,[8,9] and acute or late right heart failure.[10,11]

Biventricular failure represents an extremely ill population of patients who have end-stage heart disease that often involves both ventricles, even if its initial cause was limited to left-sided heart disease.[12] There is a high incidence of adverse events and poor 1-year survival in the biventricular VAD population.[13,14] With no linkage to any specific pump type, this condition continues to limit the long-term success of durable MCS therapies, and so demands timely intervention to sustain deteriorating hemodynamics and to facilitate symptomatic improvement.[14]

*SimuTech Group, Hudson, Ohio, †SimuTech Group, Huntsville, Alabama, ‡R1 Engineering LLC, Euclid, §Department of Biomedical Engineering, Lerner Research Institute, Cleveland Clinic, Cleveland and ¶Cleveland Clinic Lerner College of Medicine of Case Western Reserve University, Cleveland, Ohio, USA

Submitted for consideration June 2021; accepted for publication in revised form October 2021.

Disclosure: D.J.H. and K.F. are device co-inventors. The technology is owned by Cleveland Clinic. For the remaining authors, there are no conflicts of interest to disclose.

Funding: This work was supported by federal funding obtained from the National Heart, Lung and Blood Institute, National Institutes of Health, under grant 5R21HL133871.

Correspondence: Jamshid H. Karimov, MD, PhD, Department of Biomedical Engineering/ND20, Cleveland Clinic Lerner College of Medicine of Case Western Reserve University, Cleveland Clinic, 9500 Euclid Avenue, Cleveland, OH 44195, USA. E-mail: karimoj@ccf.org

DOI: 10.1097/MAT.0000000000001607

Despite major breakthroughs with MCS technology in recent years, limited efforts were made to deliver VADs with biventricular capability to clinical practice. Currently available VADs are not specifically designed for right ventricular support, which is typically limited by the LVAD operational range.[15] We are developing an innovative, advanced ventricular assist device (AVAD) which is intended to be used as a universal VAD, suitable for left heart, right heart, and biventricular support.

In this report, we present a computational flow dynamics (CFD) study of the current AVAD design to help demonstrate its intended functionality, explore the pump's self-pressure regulation feature, and identify design changes aimed at improving the pump's hydrodynamic performance that could be incorporated into the next generation design.

Materials and Methods

Device Description

The three main components of the AVAD, the housing, stator, and rotor, are shown in exploded and cross-sectional views in **Figure 1**. The pump housing was 3D printed with small holes for the static pressure taps. The internal fluid contacting surfaces of the housing were machined to remove roughness. The stator was made of titanium and the rotor was constructed of 3D printed plastic. The AVAD rotor has seven primary impeller blades, which provide the pump's hydraulic performance, and twelve secondary impeller blades, which help to maintain the pump's axial stability during operation. A thin, blood lubricated journal bearing flow path connects the primary and secondary impeller flow regions. A pressure-regulated flow restriction, or aperture, downstream of the primary impeller in combination with an axially offset volute are the key design features enabling the AVAD's biventricular capability.

The AVAD provides automatic and dynamic pump performance regulation similar to that found in our continuous-flow TAH.[16] The AVAD's rotor is free to move axially in response to varying system pressures, thereby opening or closing an aperture at the impeller discharge. This aperture functions as a differential pressure regulating valve automatically balancing the differential fluid pressure force acting on the rotor with the axial magnetic force from the motor.[17–20]

A weak magnetic force acts on the rotating assembly in the axial direction to close the aperture, while the hydraulic forces created by pump rotation act in the opposite direction to open the aperture. Should the pump rotation stop, the hydraulic forces disappear, and the axial magnetic force causes the impeller aperture to automatically close, inhibiting backflow of blood through the pump.

Operating a pump designed to be an LVAD as a right ventricular assist device (RVAD) would contribute to chronic "off-design" flow patterns of flow recirculation caused by a relatively low rotor speed for a given flow rate.[20] For the AVAD, the volute section is axially offset from the primary impeller to even out the pressures around the primary impeller providing an axisymmetric pressure and flow distribution (**Figure 1A**). This enables the AVAD to operate over a

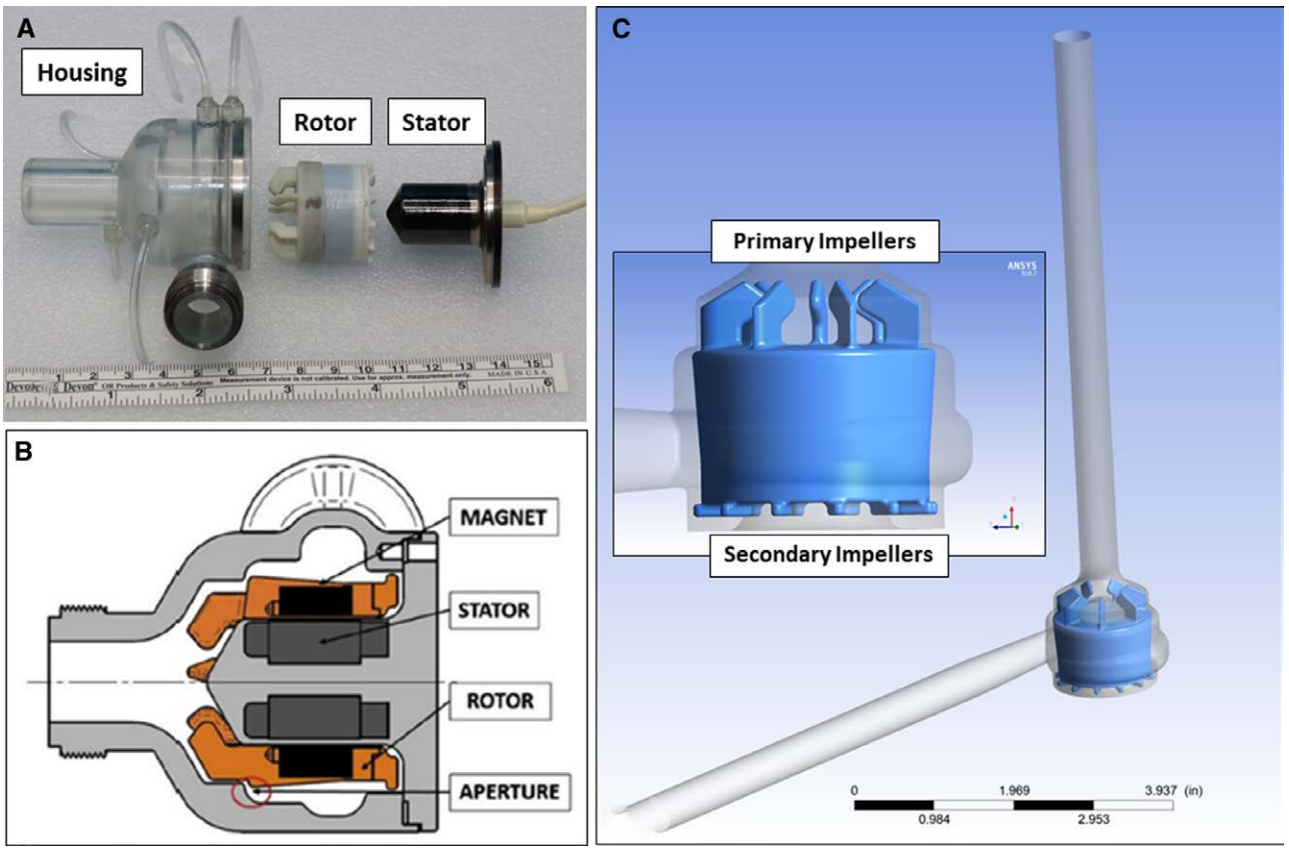

Figure 1. (A) An exploded view of the AVAD design showing the stator, rotor, and housing. (B) A cross-sectional view of the AVAD design showing the internal magnet and aperture separating the primary impeller region from the offset volute. (C) Images of the CFD model showing the extended inlet and outlet and the rotor at the nominal axial position (0.022") within the housing. full color online

wide range of flows/rotor speeds without creating adverse secondary flow patterns which could lead to thrombus formation.[21–23] This broad range of operating conditions allows the AVAD to function as either an LVAD at higher speeds/higher pressures or as an RVAD with lower speeds/lower pressures, without modification.

In Vitro Testing Description

The AVAD hydraulic performance testing was performed using a mock flow loop. In addition to the AVAD, the flow loop included manual valves for varying vascular resistance, a Transonic flow probe (Transonic Systems Inc., Ithaca, New York, USA) for measuring the flow rate, and Meritrans DTXPlus pressure transducer (Manufacturer Merit Medical, Singapore) for the pressure measurements. Polyvinyl tubing, of 3/8" inner diameter, was used to connect the flow loop components.

The testing was performed under steady-state flow conditions. A water/glycerin mixture with a density of 1060 kg/m^3 and viscosity of 2.03 centipoise was used for the testing. Static pressure measurements were recorded at the pump inlet, pump outlet, and six other locations covering each of the flow regions within the AVAD. A manifold arrangement was used to connect each of the pressure taps to the pressure transducer. For this study, the axial location of the rotating assembly was estimated photographically by viewing through a clear housing. A range of flow rates, from 2 to 8 L/min (L/min) and impeller rotational speeds, from 2300 to 3600 revolutions/min (rpm), spanning the intended use of the AVAD, were included in the testing.

CFD Model Description

Our initial focus in this CFD study was to create and validate a CFD model of the AVAD design by comparing predicted pump performance with *in vitro* measurements under steady-state flow conditions. ANSYS R18.2 (Canonsburg, Pennsylvania, USA) software, including DesignModeler, ANSYS Meshing, CFX, and CFD-Post, was used for these simulations. Images of the AVAD CFD model, with the rotor in blue, are shown in **Figure 1B**. To reduce the influence of the applied boundary conditions, six-inch-long inlet and outlet extensions were added to the pump CFD model. Leveraging the cylindrical symmetry of the pump housing surrounding both impellers, a multiframes of reference "frozen rotor" model was applied for these steady-state simulations.

The pump fluid volume was extracted from the three-dimensional AVAD model and separated into rotating and non-rotating flow domains (**Figure 2A**). The key to this effort was developing a CFD model where the different flow domains would automatically adjust and shift in response to changes in rotor axial position and aperture size. Tetrahedral mesh elements with eight prism inflation layers along all the walls were used in the volute and both impeller regions. Hexahedral mesh elements were used for the cylindrical-shaped journal bearing flow path and for the inlet and outlet extensions. The results from a mesh refinement study, conducted at the highest flow rate (8 L/min) and highest rotational speed (3600 rpm), are summarized in **Table 1**. The findings indicated very little change in the pump pressure rise (–0.4%) and impeller torque (–1.1%) between the baseline and refined mesh solutions. The refined mesh model was used for all the other simulations conducted in this study. For the refined mesh model, the prism inflation layers had an initial element height of 2.0e-04" (5.0e-03 mm) at the blade tips and 3.9e-03" (1.0 e-02 mm) on other the other impeller surfaces. Images of this refined mesh model near the primary and secondary impellers are shown in **Figure 2B**, **C**. The area-averaged mesh y+ value, which is a dimensionless distance from the wall based upon the local wall shear stress,

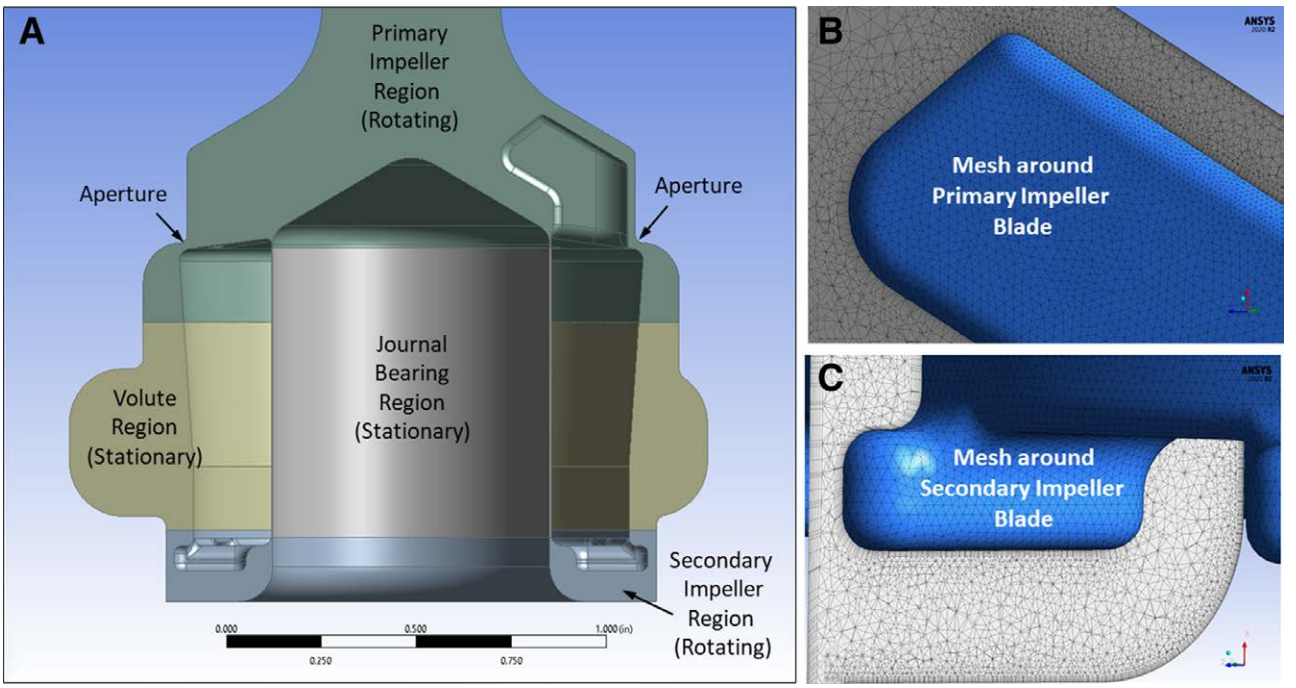

Figure 2. (A) Cross-sectional view of the different flow regions created within the AVAD with the rotor at an axial position of 0.022". (B) Cross-sectional view of the computational mesh surrounding a primary impeller blade. (C) Cross-sectional view of the computational mesh surrounding a secondary impeller blade. full color online

Table 1. Summary of the Mesh Refinement Study Results.

	Level of mesh refinement		
Mesh setting description	**Baseline mesh**	**Mid-level mesh**	**Refined mesh**
Total number of elements (millions)	**9.3**	**12.1**	**18.4**
Total number of nodes (millions)	**4.1**	**5.0**	**7.2**
Pump pressure rise (mm Hg)	**97.3**	**97.3**	**96.9**
Percentage difference from baseline	--	0.0%	-0.4%
Impeller Torque X-axis (N*m)	**–0.01425**	**–0.01430**	**–0.01409**
Percentage difference from baseline	–	0.3%	–1.1%
Impeller Maximum Yplus	**4.28**	**3.63**	**2.82**
Percentage difference from baseline	–	–17.9%	–51.8%
Impeller Area Averaged Yplus	**1.71**	**1.47**	**1.18**
Percentage difference from baseline	–	–16.3%	–44.9%

on the impeller surfaces was 1.2, with a maximum value of 2.8. These y+ values were for highest shear condition, with a flow rate of 8 L/min and impeller rotational speed of 3600 rpm. Such near-wall mesh resolution is intended to accurately capture the flow field, velocity gradients, and hence shear stress, along the walls.[24]

For the validation study, three flow rates were each modeled at four impeller rotational speeds spanning the pump's intended range of use under both RVAD and LVAD operation. A water/glycerin mixture, with fluid properties matching the *in vitro* test conditions (ρ = 1060 kg/m^3; μ = 2.03 centipoise), were used for this study. The effects of turbulent flow within the pump were captured using the Reynolds Averaged Navier Stokes shear stress transport k-ω turbulence model.[25] An average inlet static pressure and an outlet mass flow rate, matching the *in vitro* test conditions, were used as boundary conditions. The axial location of the rotating assembly, which was estimated photographically through the clear pump housing, varied by only ± 0.003″ across the range of flow conditions measured. As this degree of variation was comparable with the axial measurement resolution, we elected to position the rotating assembly at the average axial location of 0.022 for the data collected. A concentric radial location for the rotating assembly was used due to the very small bearing clearance with limited potential radial displacement of the rotor relative to the overall pump dimensions. The predicted hydraulic pressure head and wall static pressures, at six positions throughout the pump, were compared with *in vitro* experimental data to validate the CFD model. The CFD solutions were run on 12 or 16 core workstations at SimuTech Group.

With the goal of using the validated CFD model to confirm the design intent of the AVAD and identify potential design improvements, several additional studies were completed using blood. A density of 1060 kg/m^3 and a Cross non-Newtonian viscosity model,[26,27] with an infinite shear viscosity of 3.5 centipoise, was used for these blood flow simulations. We first compared the pump's flow fields under nominal RVAD and LVAD operating conditions. Then, we explored the change in pump performance with varying rotor axial positions. The intent was to evaluate the sensitivity of the pump's hydraulic performance to the aperture size. Lastly, as the pump housing was intentionally designed with a large clearance to ensure sufficient room for rotor axial movement, we evaluated the impact of reducing the secondary impeller clearance. An additional variable called "residence time", calculated using a volumetric user scalar with a source term, was included in the secondary impeller clearance simulations.

Results

CFD Model Validation

The CFD-predicted hydraulic pressure rise agreed well with the *in vitro* measured data, within 6.5% at 2300 rpm and within 3.5% for the higher rotor speeds. A plot comparing the hydraulic pressure rise test data with the CFD results is shown in **Figure 3**. Typical ranges for the flow rates and pressure increases under both RVAD and LVAD operation are also shown in this **Figure 3**. The wall static pressures, taken at six positions throughout the pump (**Figure 4A**), also agreed well with experimental data. The largest differences occurred in the primary impeller region with the CFD results underpredicting the experimental values by less than 7% for all flow/speed conditions other than at 7 L/min and 3100 rpm. At that condition, the CFD-predicted primary impeller region pressures were 10% lower than the measured values. **Figures 4B**, **C, D** show the good agreement between the CFD results and test data at the pressure tap locations over the wide range of flow/speed conditions studied. For the pressure taps in the primary and secondary impeller regions, the static pressure values from the CFD model were average values around the perimeter of the pump at the axial location of the pressure tap. The intent was to "average out" the impact of the impeller blade position relative to the pressure tap location and, in doing so, better mimic the measured "time-averaged" pressure values at those locations.

RVAD and LVAD Operation—Similarity of Flow Patterns

The intent of the aperture and the offset volute are to enable the operation of the AVAD under both RVAD and LVAD conditions. This is accomplished by providing similar flow patterns through each of the primary impeller blade passages, achieving uniformly distributed static pressures circumferentially on the impeller surfaces, and reducing flow recirculation within the volute over the wide range of RVAD/LVAD operating conditions. The images in **Figure 5A**, **B, C** show the variation in velocity in the stationary frame on a plane cutting through the primary impeller blade for the lowest, middle, and maximum operating conditions. The velocity contours show very good circumferential similarity for the blood flowing through the impeller blade passages. The images in **Figure 5D**, **E, F** show streamlines colored by velocity in the stationary frame throughout the pump. When plotting streamlines in the stationary frame they appear to pass through the impeller blades which are modeled in the rotating frame of reference. The streamline

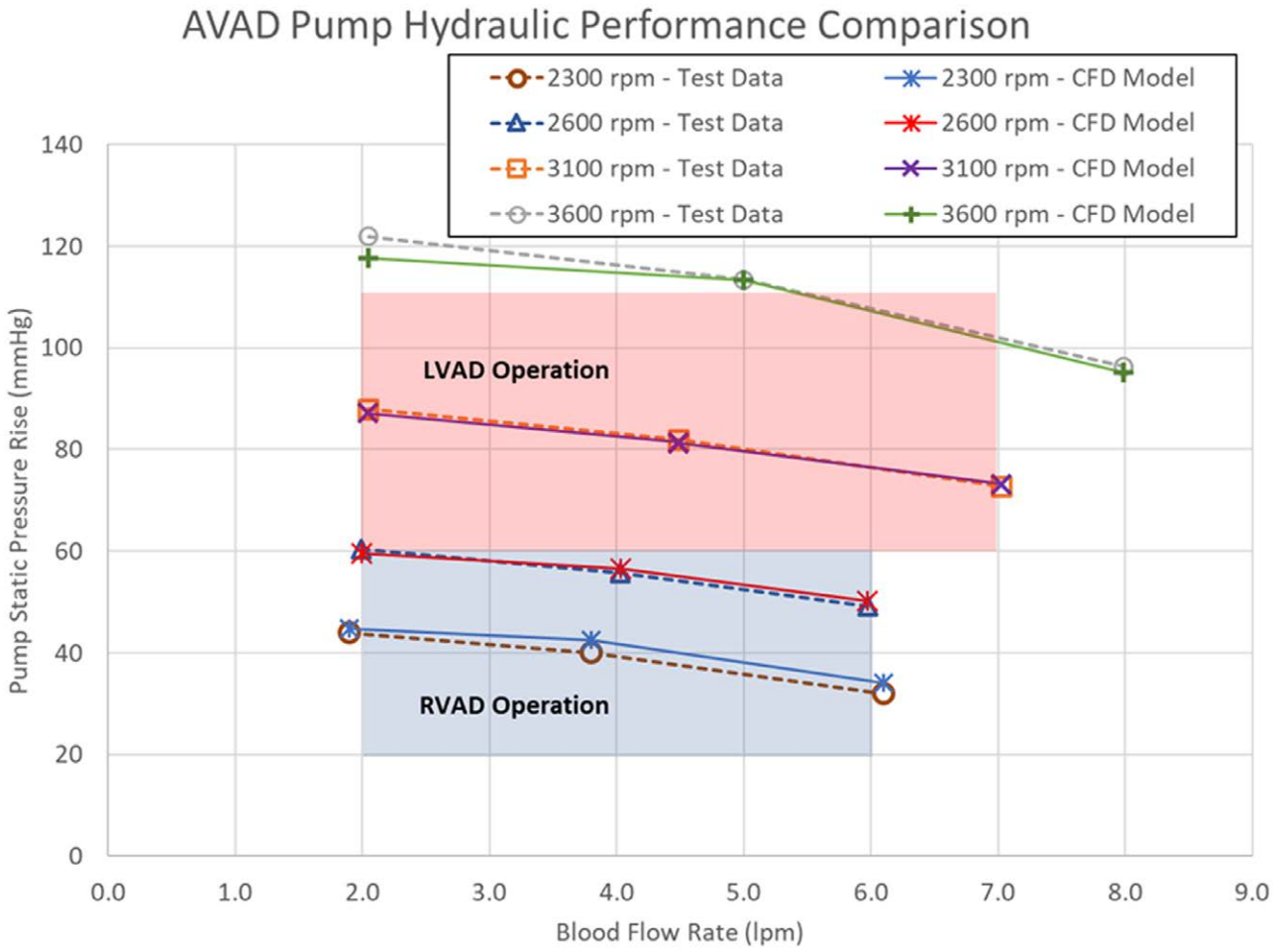

Figure 3. (A) AVAD hydraulic performance curves comparing the CFD-predicted performance with the *in vitro* measurements across the intended range of operation as both an LVAD and an RVAD. full color online

patterns throughout the pump are quite similar over this wide range of flow conditions. In addition, the absence of separated, recirculating flow within the volute region is quite promising.

Static pressure contour plots on the primary impeller surfaces (**Figure 6A**, **B, C**) and the rotating assembly surfaces (**Figure 6D**, **E, F**) show some variation in static pressure occurs on the surfaces nearest to the outlet diffuser. However, these pressure variations are small and localized helping to create a more uniform flow circumferentially around the pump. The more circumferentially uniform flow field should reduce the extent of isolated, recirculating flow regions within the offset volute region that could lead to thrombus formation.[23]

RVAD versus LVAD Comparison—Nominal Flow Conditions

In addition to comparing the flow fields within the AVAD at a nominal LVAD and RVAD flow rate of 4.5 L/min, the effect of using blood *versus* the water/glycerin mixture was also explored. The CFD results presented in **Figure 7** summarize the findings from this study.

The upper set of images in **Figure 7A**, **B, C** present velocity contours and tangential velocity vectors on a plane cutting through the primary impeller region. The velocity contours and vectors are relative to the rotating primary impeller. The velocity contours for the LVAD operation, at 3100 rpm, are extremely similar between the water/glycerin and blood solutions. Both solutions showing higher relative speeds near the center cone, where the flow enters and decreasing relative flow velocity within the blade passages, where the fluid is rotating with the blades. The flow patterns at the lower RVAD rotational speed of 2300 rpm are very similar to the LVAD results. For all these simulations, significant blade leading edge induced flow separation occurs and so reducing the blade leading edge flow incidence angle was identified as a design improvement for the next generation AVAD design.

The lower set of images in **Figure 7D**, **E, F** shows the variation in static pressure throughout the AVAD and exiting through the diffuser. The water/glycerin solution provided a slightly higher outlet static pressure than that for the blood simulation, 89.2 mm Hg *vs.* 87.5 mm Hg. The increased blood viscosity only caused a small reduction in outlet pressure because the pump is operating at a high Reynolds number and the flow is largely turbulent, when the inertial forces (velocity times density) are characteristically dominant over the viscous forces.[28] Here again, a strong circumferential similarity and uniformity of the pressure fields exist for the AVAD operating as both an LVAD and an RVAD.

Impact of Rotor Axial Position

The axial position of the rotating assembly was moved from 0.0″ to 0.089″, opening the aperture as shown in **Figure 8A**, **B**.

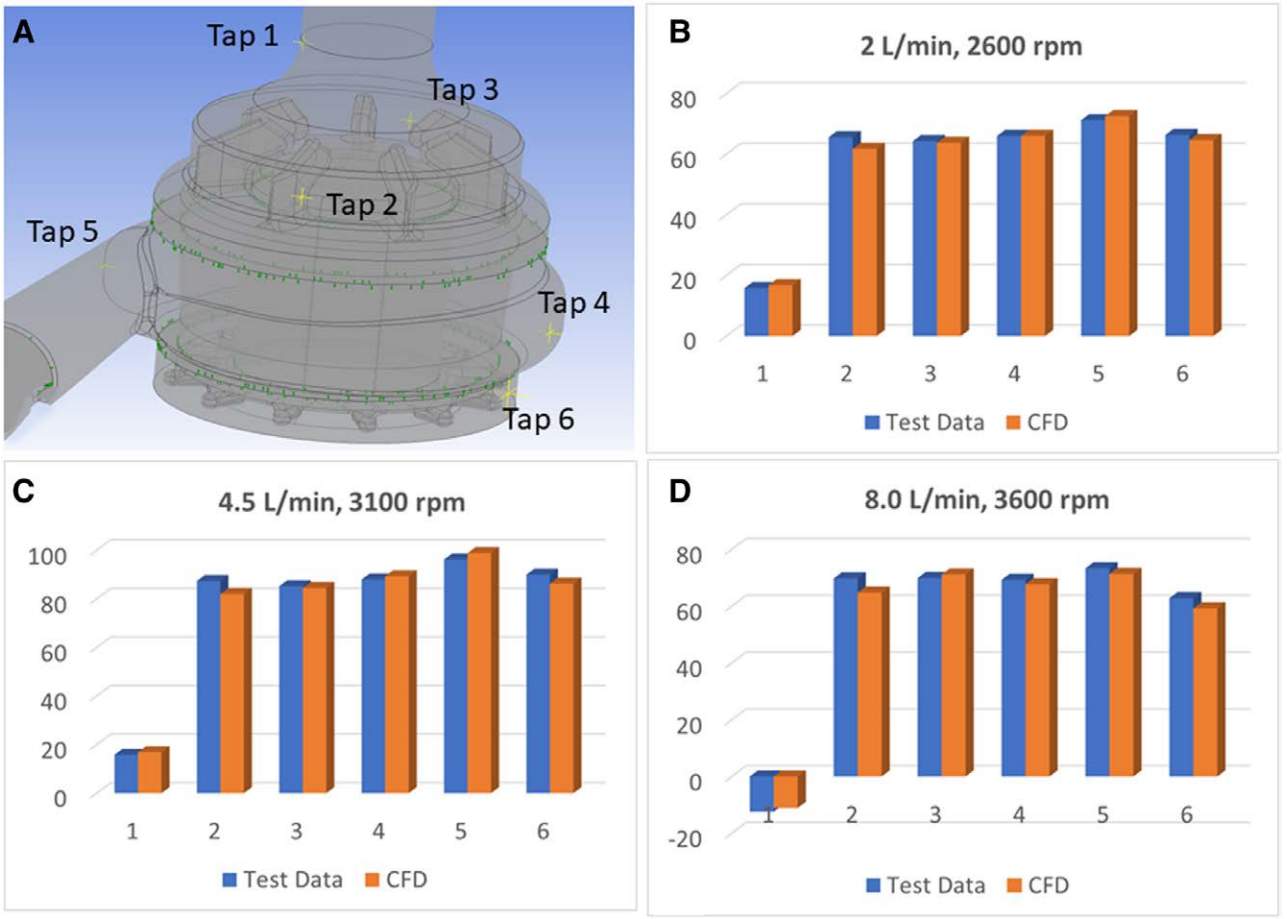

Figure 4. (A) Image showing the pressure tap locations throughout the AVAD assembly. Comparison of measured and CFD-predicted static pressures at the pressure tap locations for low flow/low speed (B), mid-flow/mid-speed (C), and high flow/high speed (D) conditions. full color online

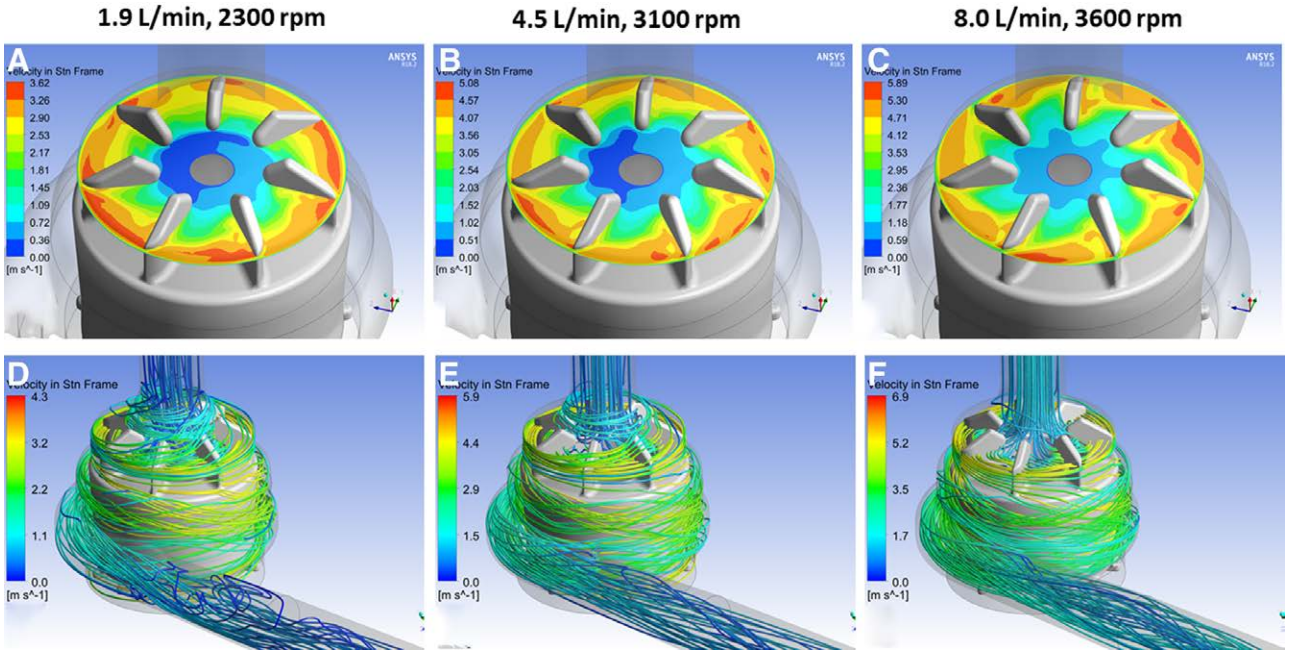

Figure 5. Contour plots of velocity in the stationary frame of reference for lowest flow/speed (A), mid-flow/speed (B), and maximum flow/speed (C) conditions showing the circumferential similarity in the flow patterns within each of the blade passages. Flow streamlines, colored by velocity in the stationary frame of reference, throughout the pump for the lowest flow/speed (D), mid-flow/speed (E), and maximum flow/speed (F) conditions. The ranges for these plots vary, based upon the local variation for each flow/speed, to better show the similarity amongst the flow conditions. full color online

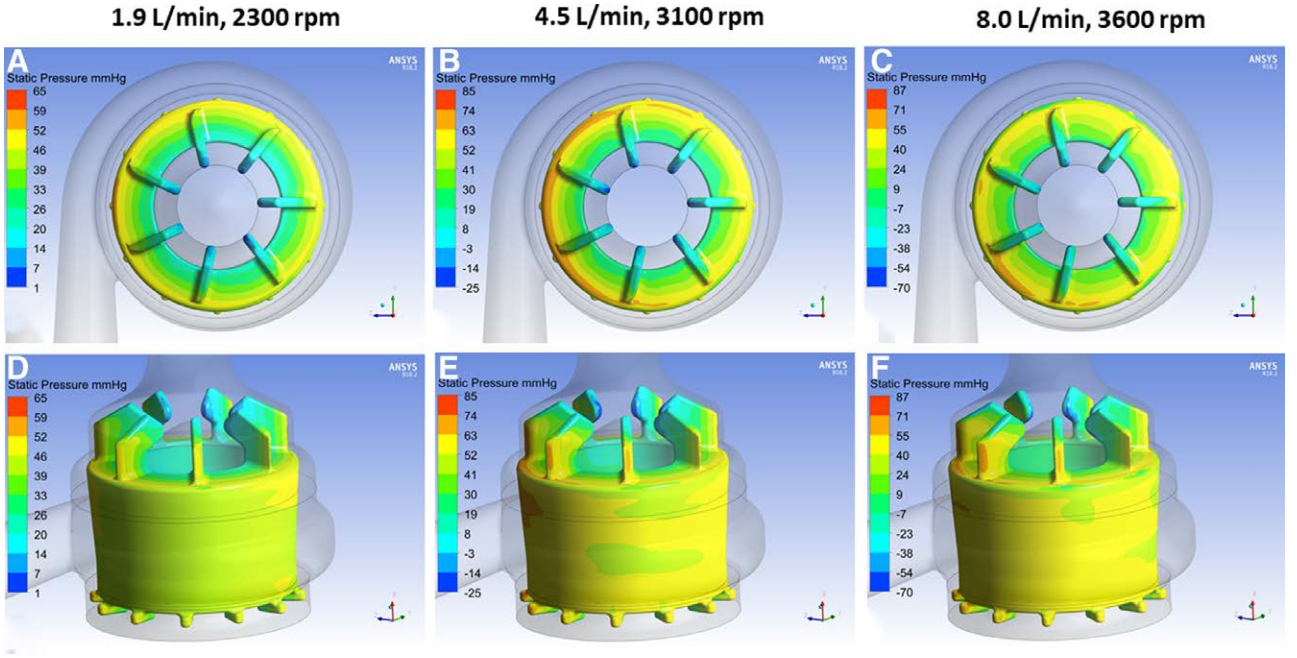

Figure 6. Contour plots of static pressure on the primary impeller face and on the entire rotating assembly at the lowest flow/speed (A, D), mid-flow/speed (B, E), and maximum flow/speed (C, F) The ranges for these plots vary, based upon the local variation for each flow/speed, to better show the similarity amongst the flow conditions. full color online

The goal of this work was to better understand the sensitivity of the pump's performance to varying the rotor axial location and aperture size. A blood flow rate of 5 L/min and rotor speed of 3400 rpm was used for this study. **Figure 8C** shows the variation in pump total pressure rise and net rotor axial force with rotor axial position. The pump total pressure rise was relatively insensitive (92–98 mm Hg) to rotor axial position over a wide range of rotor axial positions (0.015″–0.089″). As the aperture closes, the total pressure losses through the aperture increase causing the outlet pressure to decrease as intended. The net axial force

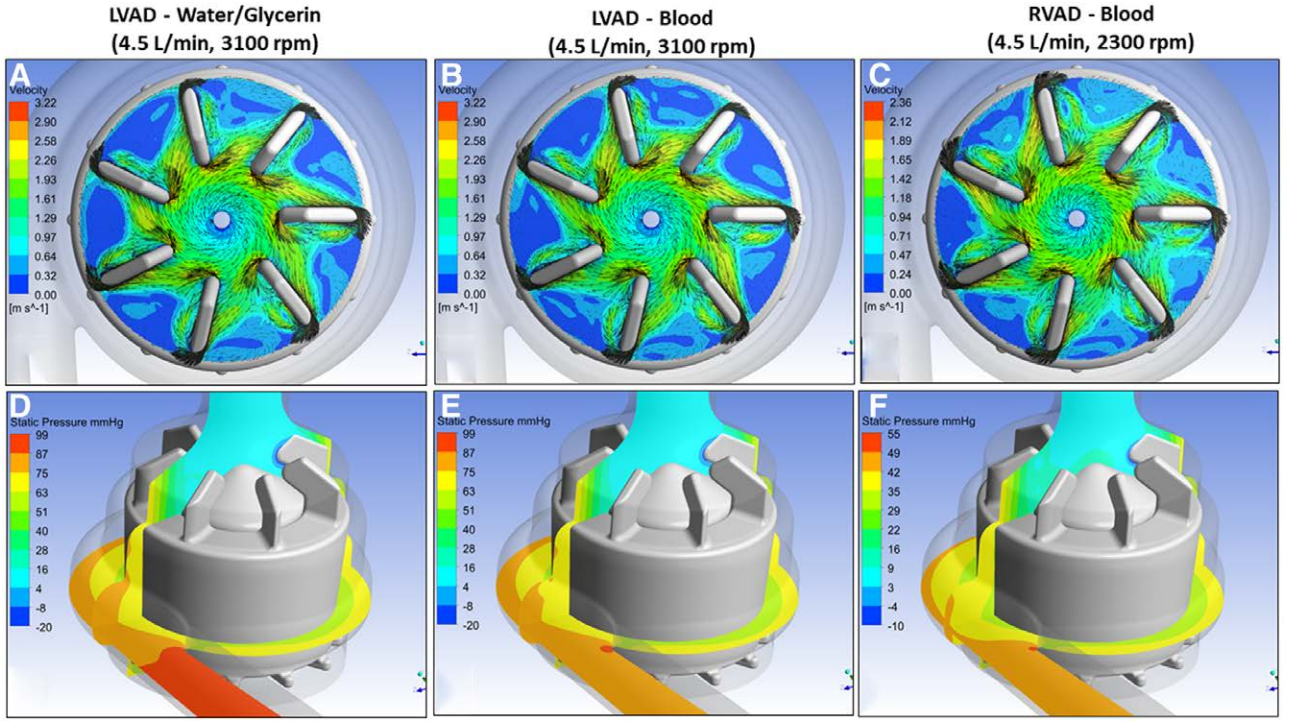

Figure 7. Images showing relative velocity contours and relative velocity vectors on a plane cutting through the primary impeller blades for nominal LVAD conditions with water/glycerin (A), blood (B), and for nominal RVAD conditions (C). These velocity values are relative to the rotating impeller. Static pressure contours indicating a small increase (1.7 mm Hg) in outlet pressure when modeling water/glycerin (D) *versus* blood (E) flow and strong axisymmetric similarity in the pressure fields when near nominal RVAD and LVAD operating conditions (E, F). full color online

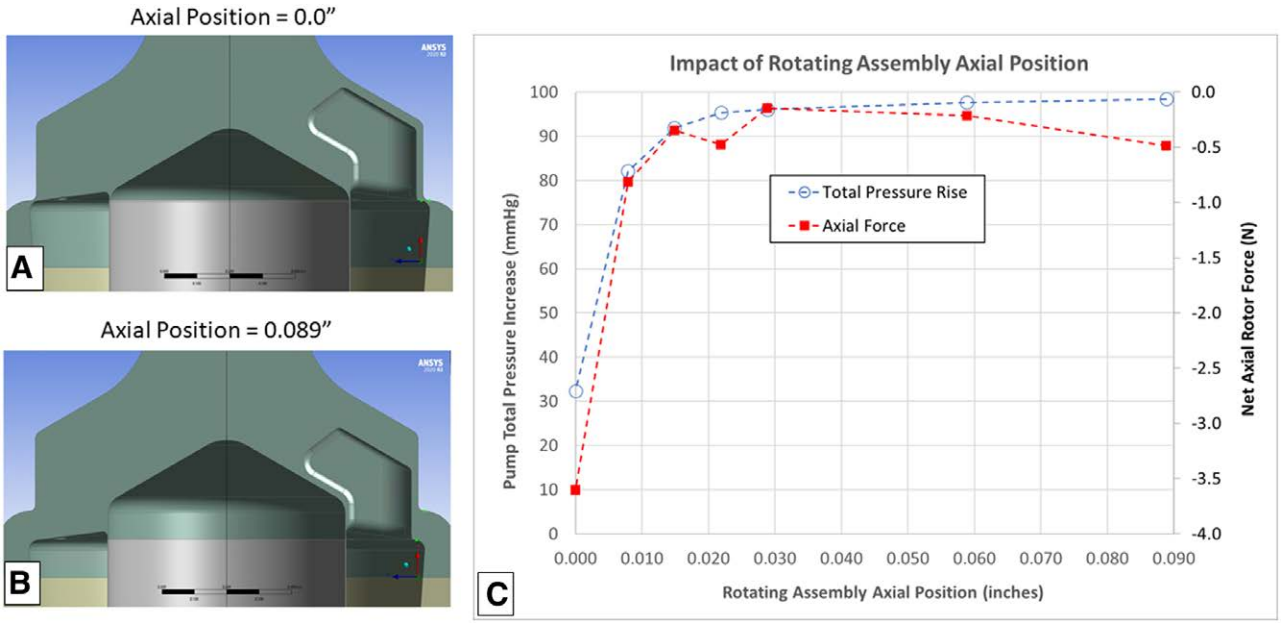

Figure 8. Cross-sectional images of the rotating assembly at axial positions of 0.0” (A) and 0.089” (B). Chart showing the variation in pump total pressure rise and net axial rotor force *versus* the axial position of the rotor, at a blood flow rate of 5 L/min and rotational speed of 3400 rpm (C). full color online

acting on the rotor is also relatively stable, with values varying between −0.15 and −0.49 N, across a wide range of rotor axial positions. These results suggest that only when the aperture begins to close, in response to system pressures, will the AVAD's hydraulic performance and axial position change significantly. Such consistency in performance and rotor axial stability, with the aperture open, was one of the initial AVAD design goals.

Reduced Secondary Impeller Clearance

In reviewing the CFD results from the nominal flow conditions study, a recirculating flow region was observed near the secondary impeller. A design modification was therefore proposed with the axial clearance in the secondary impeller region reduced by 0.394” (1 mm). The intent was twofold: (1) to remove excess flow volume in that region, to reduce the extent of the observed flow recirculation, and (2) to reduce the secondary impeller pressure, encouraging increased rotor axial movement. Such increased sensitivity in axial movement with rotor speed would help differentiate LVAD from RVAD operation. A blood flow rate of 4.5 L/min, rotor speed of 3100 rpm, and a rotor axial location of 0.022” was used for this study. The smaller secondary clearance reduced the volume-averaged residence time in the secondary impeller region by 10%. A lower average flow residence time indicates improved washout with less flow recirculation near the secondary impeller. Such improved flow patterns should reduce the likelihood of thrombus forming near the secondary impeller.[24] Contour plots comparing flow residence times within the secondary impeller regions are shown in **Figures 9A**, **B**. With the aperture isolating the two impeller regions, the reduced secondary clearance had negligible impact on the pump's hydraulic pressure rise (−0.2 mm Hg). Reducing the clearance increases the local speed along the inner surfaces of the secondary impeller, specifically near the journal bearing connection. This localized speed increase is accompanied by a reduction in the static pressure near the inside of the secondary impeller as shown in **Figures 9C**, **D**. Lower secondary impeller pressures reduce the rotor net axial force from −0.16N to −0.30N, providing increased axial movement of the rotor in response to varying pressure differences. This increased responsiveness is desired and could improve the responsiveness and pulsatility in the pump's operation.

Discussion

For end-stage heart failure, heart transplantation or implantation of a left ventricular assist device (LVAD) is lifesaving and provides a significant improvement in quality of life.[2,3] Despite the therapeutic success of LVADs,[4] concomitant right ventricular failure (RVF) and the lack of appropriate long-term, right ventricular (RV) support devices have limited the full potential that mechanical circulatory support (MCS) can offer to patients with biventricular failure.[29–32] Despite the relatively low rate of temporary right ventricular assist device (RVAD) support in the US, a significant number of patients who have been successfully discharged after receiving an LVAD remain symptomatic from RVF and undergo recurrent readmissions for management of heart failure. In addition, delayed RVF is being increasingly recognized in a subset of patients on chronic LVAD support. Therefore, it is imperative that newer technologies designed or adapted for RV support be developed.

Due to less apparent clinical demand for RVADs than for LVADs,[33] the durable MCS devices have not been designed specifically for RVAD application. The resulting lack of a reliable RVAD further diminishes the treatment options for patients with biventricular failure or those with isolated and post-LVAD RVF.[34–37]

RVAD pumps operate at much lower afterloads (pulmonary arterial pressure) than those of LVADs and at significantly lower hydraulic loads and power consumption rates. A challenging

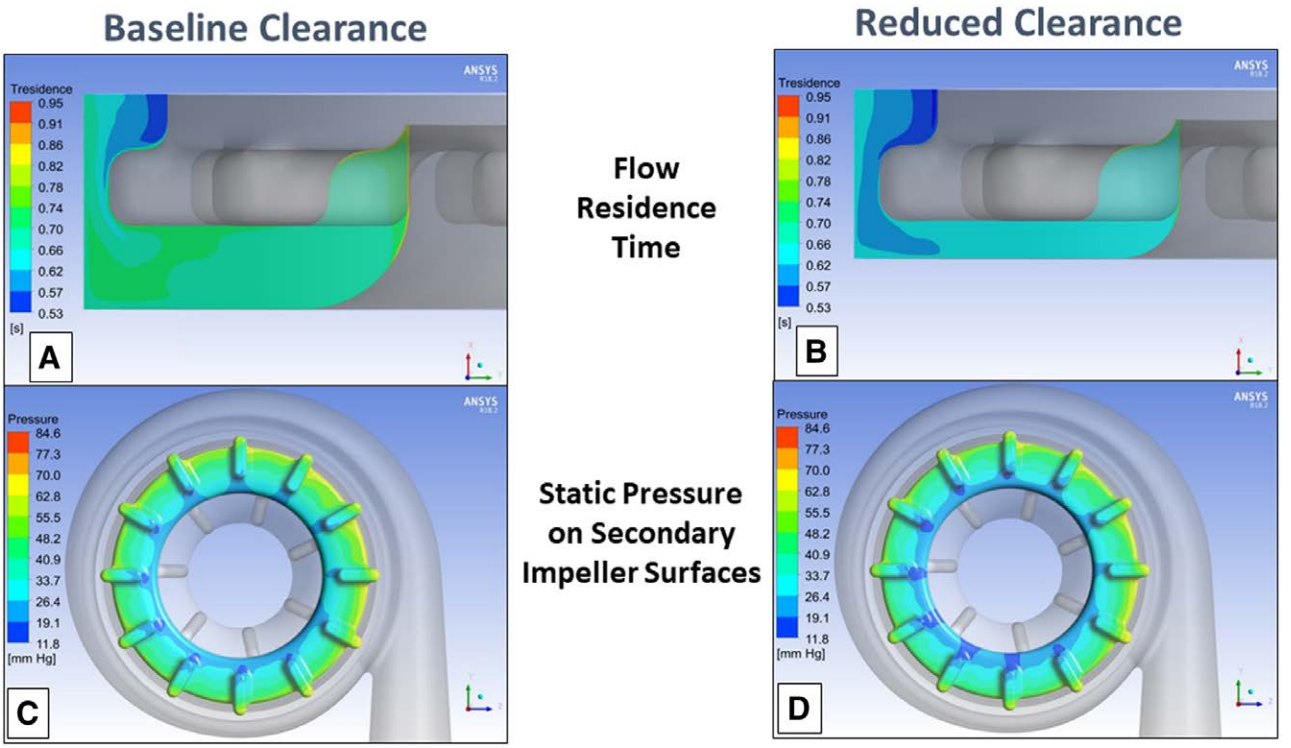

Figure 9. Contour plots of residence time within the secondary impeller flow region are shown for the baseline (A) and reduced-axial clearance (B) designs. In addition to reducing flow residence time, the reduced axial clearance also reduces the static pressures near the inner surfaces of the secondary impeller (C, D). full color online

design issue arises when considering both the maximum speed needed to meet the LVAD range and the minimum speed needed for the RVAD range, which results in a speed ratio of 2.5:1 for a combined LVAD/RVAD pump's operating range. If an LVAD with a pump flow of 5 L/min at 80 mm Hg of pump pressure rise (differential pressure) is used as an RVAD, pump flow increases to >11 L/min due to much lower pump pressure rise (30 mm Hg, as an example) in the pulmonary circulation. The question of left and right balancing in CF biventricular configurations has been discussed but remains debatable.[38] The right and left ventricles generate different hemodynamic profiles. This is important from a technical standpoint during surgery as well as for the management of both devices during long-term biventricular assistance to prevent pulmonary overflow and development of pulmonary edema. As a result, often modifications are necessary for current LVADs intended for RVAD use, as devices would generate different flow rates due to variances in RV and LV filling pressures and variances in systemic vascular resistance *vs.* pulmonary vascular resistance.

A unique aspect of the universal AVAD currently undergoing development at the Cleveland Clinic is that its rotor moves axially in response to varying system pressures, opening or closing an aperture at the right impeller discharge. This aperture functions as a differential pressure regulating valve automatically balancing the differential fluid axial pressure force acting on the rotor. The aperture also provides a flow restriction that limits the right pump discharge pressures yet maintains the desired higher left pump discharge pressures. Also, the negative effects expected with graft narrowing are fully omitted with the AVAD, therefore improving the outflow graft hemodynamics aimed at reducing the likelihood of downstream thrombus formation.

This CFD study was completed to supplement experimental testing in helping to demonstrate the biventricular operation and to explore design sensitivities of this new, advanced ventricular assist device (AVAD). The overall intent of the work was to gain insight into the flow fields within the AVAD over a wide range of operating conditions. With such additional insight, we would be able to visualize the similarity of the internal pump flows when operating as an RVAD and an LVAD to confirm the pump's design intent and identify design changes aimed at improving the pump's hydraulic performance and/or biocompatibility.

To accomplish these goals, we first performed a validation study of the AVAD CFD model. The benefits of performing this study were twofold. First, we established the credibility of the CFD model results by predicting the static pressures throughout the pump. This provided a platform for us to conduct virtual design studies to assess the sensitivity of the pump's hydraulic performance to rotor axial position (aperture size) and to explore a proposed change in the secondary impeller clearance. Second, by comparing the simulations with the measured static pressure values across the broad range of intended AVAD operating conditions, we gained insight into the ability of the pump to function as either an RVAD or an LVAD. Being able to visualize the similarity and circumferential uniformity of the internal flow fields across the AVAD's intended operating conditions supported the theory upon which the pump design was based. That was to create a pump that automatically responds to varying afterload conditions without causing adverse, recirculating flows at off-design conditions.

The AVAD's unique offset volute design provided an axisymmetric geometry surrounding both the primary and secondary impellers. This axisymmetric geometry not only simplified the

CFD modeling approach, being able to apply the steady-state frozen rotor model but also reduced the influence of the diffuser location on the pressure and flow uniformity throughout the volute. The offset volute, in combination with the pressure-regulating aperture, yielded flow fields within the primary impeller region that were nearly axisymmetric across the flow rates and impeller speeds studied. Such circumferential flow uniformity significantly reduces secondary, recirculating flow patterns within the volute and impeller that were observed when using other VADs operating at "off-design" conditions for a right ventricular assist.[20] Minimizing the secondary, recirculating flow regions reduces the likelihood of thrombus forming within the pump. We also observed consistent flow separation originating from the leading edges of the primary impeller blades. For the next generation AVAD design we plan to adjust the leading-edge blade angle to reduce the blade incidence angle and resulting tip-induced flow separation.[39]

The validation study was performed with a water/glycerin mixture. The additional studies, varying axial rotor location and secondary impeller clearance, were conducted using non-Newtonian blood. To assess the impact of having a different fluid viscosity, we performed a study at a nominal flow rate of 4.5 L/min and rotor speed of 3100 rpm. The results revealed very similar flow fields throughout the pump with a slightly higher pressure rise, of 2%, for the water/glycerin mixture. As the flow within the pump is inertially driven, it seemed most important to match the test and blood density values. The blood's increased viscosity had only a small, secondary impact on the pump's performance and flow patterns.

The AVAD rotor responds automatically, moving axially, in response to the varying downstream pressure. This rotor movement opens or closes the aperture in response to the changing downstream flow resistance. We conducted a study to evaluate the sensitivity in the pump's hydraulic performance in response to the rotor axial position. The results from this study revealed relatively constant pump pressure rise over a wide range of rotor axial positions, from 0.015" to 0.089". Then, as the aperture closes, the pressure rise drops quickly as intended to shut off the flow should a sudden decrease in downstream pressure occur.

The results also indicate a low meridional speed through the impeller blades that brings unnecessary residence time and flow recirculation. A large blade height was included in the original design to help ensure meeting the desired hydraulic performance of the pump. An improvement can likely be realized with investigation of a reduced primary impeller blade height, which would allow a smaller volume surrounding the primary impeller and decrease the residence time and extent of recirculating flows in this region. Both effects would likely improve the biocompatibility of the pump, as well as reduce power consumption. Determining the impact of a reduced primary blade height on the overall pump's performance will be explored for the next generation AVAD design.

When reviewing the flows surrounding the secondary impeller, we noticed recirculating flow patterns. Such recirculating flows indicate an excess of flow volume in this region. As mentioned earlier, the axial clearance for this initial AVAD design was intentionally oversized to provide sufficient room for rotor axial movement to ensure the pump's functionality. Therefore, we decided to explore the impact of reducing the secondary impeller clearance by 0.39" (1 mm). Reducing the axial clearance resulted in a 10% reduction in average residence time in the secondary impeller region. This change also reduced the static pressures near the center of the secondary impeller which reduced the upward forces on the rotor. The reduction in the axial stiffness, resulting from the secondary impeller pressure force, could be beneficial in providing more responsiveness and pulsatility in the pump's operation. Both effects would be desirable, and this housing change has been included in the next generation AVAD design.

Limitations

One limitation of the current study is the limited resolution of the rotor axial position measurement. The optical method used indicated very small changes in the rotor axial position (± 0.003") over the range of flow conditions studied. Incorporating a position sensor capable of resolving and providing a time-averaged axial rotor location would allow us to prescribe different axial positions for each flow/rotor speed condition. In addition, more accurate position sensing would support in-depth CFD studies focused on the AVAD's performance as the aperture closes.

Another limitation was that the CFD studies were all performed under steady-state flow conditions. Under actual operation, the pressures, flow rate, and rotor axial position of the AVAD would be continuously varying. In addition, the left and right ventricular contractility and the associated interactions with the AVAD would also be changing with time. The time scale related to the rotor spinning at 2300 to 3600 rpm (7e-05 to 4.6e-05 sec for 1° of rotation) is significantly smaller than the time scale associated with these pulsatile blood flow transient conditions (~1 sec). This, combined with the lack of precise information related to the rotor axial placement, makes transient solutions not practical for this initial study. To address this limitation, we elected to capture the variation in operating conditions and rotor axial position through a series of separate steady-state simulations. Our expectations are that the trends and insight gained from the steady-state simulations will be applicable to the actual, transient operation of the AVAD.

One other limitation is that we only evaluated the change in hydraulic performance with change in rotor axial position at one set of flow conditions (5 L/min, 3100 rpm). These conditions were near the nominal rotor speed value for LVAD operation. Future work will evaluate the sensitivity of pump performance to rotor axial position over a broader range of blood flow rates and impeller speeds.

Conclusions

In summary, we conducted a CFD study that investigates the unique design aspects of the AVAD and further supports its functionality as a biventricular assist device. By comparing *in vitro* pressure measurements throughout the pump, we demonstrated the validity of the AVAD CFD model over a wide range of operating conditions applicable to both left and right ventricular support. Through these simulations we showed the similarity and circumferential uniformity of the flow field within the primary impeller region needed for biventricular operation. The pressure-regulated aperture, in combination with an offset volute, were the key features enabling such well-distributed flows over such a wide range of conditions. Having well-distributed flows

throughout the pump reduces the extent of undesired, secondary flow patterns that can lead to thrombus formation.

The CFD analyses were also used to better understand the operation and identify potential improvements to the initial AVAD design. The sensitivity in the pump's hydraulic performance with varying aperture size, *i.e.,* rotor axial position, was demonstrated. The hydraulic performance of the AVAD remained nearly constant over a wide range of aperture sizes, then decreased quickly as the aperture started closing. This behavior is consistent with the shut-off capabilities of the pump. Several potential changes to further improve the hydrodynamic performance and biocompatibility of the AVAD included: (1) increasing the leading-edge curvature of the primary impeller blade to reduce tip-induced flow separation, (2) reducing the primary impeller blade height and clearance to increase the pump's pressure responsiveness and reduce flow residence time, and (3) reducing the secondary impeller clearance to again increase the pump's pressure responsive and reduce flow residence time. The intent in reducing flow residence time is to minimize regions of recirculating flow that could lead to thrombus formation.

Overall, the CFD results supported prior studies demonstrating and helping to visualize the unique aspects of the AVAD. Future studies will build upon this work to aid in assessing the proposed design refinements of this innovative biventricular assist device.

Acknowledgements

This work was supported with federal funding obtained from the National Heart, Lung and Blood Institute, National Institutes of Health (NHLBI), under grant 5R21HL133871.

References

1. Ambrosy AP, Fonarow GC, Butler J, *et al*: The global health and economic burden of hospitalizations for heart failure: Lessons learned from hospitalized heart failure registries. *J Am Coll Cardiol* 63: 1123–1133, 2014.
2. Garbade J, Bittner HB, Barten MJ, Mohr FW: Current trends in implantable left ventricular assist devices. *Cardiol Res Pract* 2011: 290561, 2011.
3. Wever-Pinzon O, Drakos SG, Kfoury AG, *et al*: Morbidity and mortality in heart transplant candidates supported with mechanical circulatory support: Is reappraisal of the current United network for organ sharing thoracic organ allocation policy justified? *Circulation* 127: 452–462, 2013.
4. Moazami N, Hoercher KJ, Fukamachi K, *et al*: Mechanical circulatory support for heart failure: Past, present and a look at the future. *Expert Rev Med Devices* 10: 55–71, 2013.
5. Pak SW, Uriel N, Takayama H, *et al*: Prevalence of de novo aortic insufficiency during long-term support with left ventricular assist devices. *J Heart Lung Transplant* 29: 1172–1176, 2010.
6. Bartoli CR, Zhang D, Kang J, *et al*: Clinical and *In Vitro* evidence that subclinical hemolysis contributes to LVAD thrombosis. *Ann Thorac Surg* 105: 807–814, 2018.
7. Starling RC, Moazami N, Silvestry SC, *et al*: Unexpected abrupt increase in left ventricular assist device thrombosis. *N Engl J Med* 370: 33–40, 2014.
8. Sunagawa G, Byram N, Karimov JH, *et al*: The contribution to hemodynamics even at very low pump speeds in the HVAD. *Ann Thorac Surg* 101: 2260–2264, 2016.
9. Sunagawa G, Byram N, Karimov JH, *et al*: *In vitro* hemodynamic characterization of HeartMate II at 6000 rpm: Implications for weaning and recovery. *J Thorac Cardiovasc Surg* 150: 343–348, 2015.
10. Anderson M, Morris DL, Tang D, *et al*: Outcomes of patients with right ventricular failure requiring short-term hemodynamic support with the Impella RP device. *J Heart Lung Transplant* 37: 1448–1458, 2018.
11. Takeda K, Takayama H, Colombo PC, *et al*: Late right heart failure during support with continuous-flow left ventricular assist devices adversely affects post-transplant outcome. *J Heart Lung Transplant* 34: 667–674, 2015.
12. Dandel M, Krabatsch T, Falk V: Left ventricular vs. biventricular mechanical support: Decision making and strategies for avoidance of right heart failure after left ventricular assist device implantation. *Int J Cardiol* 198: 241–250, 2015.
13. Shah P, Ha R, Singh R, *et al*: Multicenter experience with durable biventricular assist devices. *J Heart Lung Transplant* 37: 1093–1101, 2018.
14. Vierecke J, Gahl B, de By TMMH, *et al*: Results of primary biventricular support: An analysis of data from the EUROMACS registry. *Eur J Cardiothorac Surg* 56: 1037–1045, 2019.
15. Karimov JH, Sunagawa G, Horvath D, Fukamachi K, Starling RC, Moazami N: Limitations to chronic right ventricular assist device support. *Ann Thorac Surg* 102: 651–658, 2016.
16. Horvath DJ, Karimov JH, Byram NA, *et al*: Advantages of integrating pressure-regulating devices into mechanical circulatory support pumps. *ASAIO J* 65: e1–e3, 2019.
17. Miyamoto T, Byram N, Karimov JH, *et al*: The design modification of advanced ventricular assist device to enhance pulse augmentation and regurgitant flow shut-off. *Artif Organs* 43: 961–965, 2019.
18. Miyamoto T, Kado Y, Horvath DJ, *et al*: An advanced universal circulatory assist device for left and right ventricular support: First report of an acute in vivo implant. *JTCVS Open* 3: 140–148, 2020.
19. Karimov JH, Horvath D, Horvath D, *et al*: Mechanical circulatory support for biventricular heart failure using advanced ventricular assist device. *J Heart Lung Transpl* 39: S414, 2020.
20. Fukamachi K, Horvath DJ, Byram N, Sunagawa G, Karimov JH, Moazami N: Advanced ventricular assist device with pulse augmentation and automatic regurgitant-flow shut-off. *J Heart Lung Transplant* 35: 1519–1521, 2016.
21. Bluestein D, Niu L, Schoephoerster RT, Dewanjee MK: Fluid mechanics of arterial stenosis: Relationship to the development of mural thrombus. *Ann Biomed Eng* 25: 344–356, 1997.
22. Sheriff J, Bluestein D, Girdhar G, Jesty J: High-shear stress sensitizes platelets to subsequent low-shear conditions. *Ann Biomed Eng* 38: 1442–1450, 2010.
23. Chiu WC, Slepian MJ, Bluestein D: Thrombus formation patterns in the HeartMate II ventricular assist device: Clinical observations can be predicted by numerical simulations. *ASAIO J* 60: 237–240, 2014.
24. *ANSYS-CFX Modeling Guide C, Turbulence and Near-Wall Modeling, Modeling Flow near the Wall, Version R18.2*.
25. Menter FR: Two-equation eddy-viscosity turbulence models for engineering applications 32:1598–1605, 1994.
26. Cross MM: Rheology of Non-Newtonian Fluids—A New Flow Equation for Pseudoplastic Systems. *J Colloid Sci* 20: 417–437, 1965.
27. Banerjee RK CY, Kensey K: Effect of non-Newtonian viscosity of blood on steady and pulsatile flow in stenosed arteries. *Adv Bioeng* 20: 103–106, 1991.
28. Day SW, Lemire PP, Flack RD, McDaniel JC: Effect of Reynolds Number on Performance of a Small Centrifugal Pump ASME/JSME 2003 4th Joint Fluids Summer Engineering Conference, 2003:1893–1899.
29. Fukamachi K, McCarthy PM, Smedira NG, Vargo RL, Starling RC, Young JB: Preoperative risk factors for right ventricular failure after implantable left ventricular assist device insertion. *Ann Thorac Surg* 68: 2181–2184, 1999.
30. Kukucka M, Stepanenko A, Potapov E, *et al*: Right-to-left ventricular end-diastolic diameter ratio and prediction of right ventricular failure with continuous-flow left ventricular assist devices. *J Heart Lung Transplant* 30: 64–69, 2011.
31. Simon MA: Assessment and treatment of right ventricular failure. *Nat Rev Cardiol* 10: 204–218, 2013.
32. Steffen RJ, Halbreiner MS, Zhang L, *et al*: Mechanical circulatory support for the right ventricle in the setting of a left ventricular assist device. *Expert Rev Med Devices* 11: 587–593, 2014.
33. Fukamachi K, Shiose A, Massiello AL, *et al*: Implantable continuous-flow right ventricular assist device: Lessons learned in the development of a cleveland clinic device. *Ann Thorac Surg* 93: 1746–1752, 2012.

34. Moazami N, Fukamachi K, Kobayashi M, *et al*: Axial and centrifugal continuous-flow rotary pumps: A translation from pump mechanics to clinical practice. *J Heart Lung Transplant* 32: 1–11, 2013.
35. Loforte A, Stepanenko A, Potapov EV, *et al*: Temporary right ventricular mechanical support in high-risk left ventricular assist device recipients versus permanent biventricular or total artificial heart support. *Artif Organs* 37: 523–530, 2013.
36. Kaczorowski DJ, Woo YJ: Who needs an RVAD in addition to an LVAD? *Cardiol Clin* 29: 599–605, 2011.
37. Timms D, Gude E, Gaddum N, *et al*: Assessment of right pump outflow banding and speed changes on pulmonary hemodynamics during biventricular support with two rotary left ventricular assist devices. *Artif Organs* 35: 807–813, 2011.
38. Bartoli CR, Dowling RD: The future of adult cardiac assist devices: Novel systems and mechanical circulatory support strategies. *Cardiol Clin* 29: 559–582, 2011.
39. Davis MJAJ: Design of flat plate leading edges to avoid flow separation. 18: 598–600, 1980.